Demonstration of Sub-THz Traveling-Wave Resonant-Tunneling-Diode Oscillators

Zoltán Jéhn and Michael Feiginov

***Abstract*—As a proof of principle, operation of traveling-wave resonant-tunneling-diodes (RTDs) oscillators has been demonstrated experimentally in the frequency range 100-400 GHz. A theoretical model describing a realistic coupled system, consisting of a traveling-wave RTD and a patch antenna, has been developed. The model describes the eigen resonances and the eigen modes, which have a mixed character of both subsystems. The model and the experimental results are in agreement with each other. We also demonstrate that some oscillators were switching between different resonant modes of the system with the change of bias. The phenomenon could be used for an extended frequency control of the RTD oscillators.**

***Index Terms*—Measurement, modeling, oscillators, resonant-tunneling diodes (RTDs), resonators.**

Nomenclature

Symbol	*Description and unit*
$\omega,\ f$	Angular frequency and frequency [s^{-1}].
k	Propagation constant in the waveguide [1/m].
Z	Wave impedance of the waveguide [Ω].
L	Line inductance of the waveguide [H m^{-1}].
R_{metal}	Line resistance of the metal layer [Ω m^{-1}].
C_{RTD}, c_{RTD}	RTD line and areal capacitance [F/m, F/m^2].
G_{RTD}, g_{RTD}	RTD line and areal conductance [S/m, S/m^2].
r_c	Areal contact resistance [Ω m^2].
σ	Conductivity of the metal [S m^{-1}].
σ_{n++}	Conductivity of the n++ layer [S m^{-1}].
w	Width of the waveguide [m].
l	Length of the waveguide [m].
l_{ant}	Length of the antenna [m].
d_{wg}	Spacing between the metal waveguide plates [m].
d_{n++}	Thickness of the n++ layer [m].
ϵ	Dielectric constant [F m^{-1}].
μ_0	Vacuum permeability [H m^{-1}].
d_{sk}	Skin depth [m].
d_{bar}	RTD barrier thickness [m].
G_{n++}	Line conductance of the n++ layer [S m^{-1}].
C_{n++}	Line capacitance of the n++ layer [F m^{-1}].
G_{cont}	Line conductance of the contact layer [S m^{-1}].
C_{cont}	Line capacitance of the contact layer [F m^{-1}].
$P_+,\ P_-$	Power emitted from the waveguide at its ends [W].
P_{rad}	Radiated power from the antenna [W].

Abbreviations

RTD	Resonant tunneling diode.
TLM	Transmission line method.
MIM	Metal-insulator-metal.
n++	Heavily doped semiconductor semiconductor layer.
CPW	Coplanar waveguide.
PP	Parallel plate.

Manuscript received 4 January 2023; accepted 3 February 2023. Date of publication 9 February 2023; date of current version 21 February 2023. The work was supported in part by the European Union's Horizon 2020 Research and Innovation Program under the Marie Sklodowska-Curie under Grant 765426 (TeraApps), in part by CzechNanoLab Project LM2018110 funded by MEYS CR support for the measurements/sample fabrication at CEITEC Nano Research Infrastructure, and in part by TU Wien Bibliothek through its Open Access Funding Programme. The review of this article was arranged by Associate Editor J. Han. *(Corresponding authors: Zoltán Jéhn; Michael Feiginov.)*

The authors are with the Department of Electrical Engineering, Information Technology, TU Wien, 1040 Vienna, Austria (e-mail: jehn.zoltan@gmail.com; michael.feiginov@tuwien.ac.at).

Digital Object Identifier 10.1109/TNANO.2023.3243462

I. Introduction

THE terahertz frequency range remains an intensive research area in the last decades. Nowadays, a number of different devices and systems exist, that can operate in this frequency range, expanding from the microwave to infrared frequencies. The most prominent examples of the semiconductor structures that can operate in the higher bounds of this frequency range are the quantum cascade structures (QCLs) [1], [2], and in the lower bounds are the resonant-tunneling-diodes (RTDs) oscillators [3], [4], [5], [6], [7], HEMT (high-electron-mobility transistor) amplifiers [8], Gunn diodes [9], (impact avalanche transit time diodes) IMPATT diodes [10] and Schottky diodes as detectors and multipliers [11].

The operation at room temperature and relative simplicity gives advantages to RTD oscillators compared to the other types of THz sources [4], [5]. In fact, RTDs are the highest-frequency active semiconductor devices nowadays, their operating frequency has reached almost 2 THz [6], [7]. However, the output power of RTD oscillators remains rather low so far, it is in the range of few tens of μW at THz frequencies and above [4], [5], [12]. For this reason and also in view of limited tunability of RTD oscillators [13], the investigation of different configurations and concepts of RTD oscillators remains an active research field. The RTDs oscillators are usually based on a lumped-element oscillator concept. However, some time ago a concept of traveling-wave (TW) RTD oscillator has been put forward and it was shown to be (theoretically) feasible [14]. In the present paper, we investigate a practical realization of TW RTD oscillators: a TW RTD needs to be coupled to an external

(passive) emitting antenna, which basically together with the TW part creates a system of two coupled resonators. The analysis of the oscillation conditions of such coupled systems is one of the objectives of the paper. The second objective is the experimental proof-of-principle demonstration of such TW RTD oscillators. Additionally, we have found out that our TW RTD oscillators could be switched between different oscillation modes by changing the RTD bias; that gives additional degrees of freedom to control the oscillation frequency of RTD oscillators or to modulate them.

II. Device Structure

A TW oscillator can be constructed from a waveguide integrated with negative differential conductance (NDC) layers along it [15]. The gain of the NDC layers, RTD layers in our case, should be sufficiently high to compensate for the waveguide losses. If the waveguide is long compared to the wavelength of the waveguide modes, then the modes will be bouncing back and forth between the end facets of the waveguide, such an oscillator will work similar to a laser. In a realistic situation, however, there are two essential differences. First, the waveguide is not much longer than the wavelength of the waveguide modes. Its length is either smaller or, in the best case, comparable to the wavelength. Second, the waveguide is coupled to the emitting antenna, which has its own resonant properties. Therefore, the resonant cavity of the oscillator includes not only the TW part, but also the antenna resonator. That is a system with coupled resonators. Such coupled system can have different operation modes. In some cases, the system operates closer to a TW oscillator regime (the wavelength is comparable to the length of the TW part). In other cases, the wavelength is smaller and can be even much smaller than the length of the TW part, then the system works closer to a lumped-element oscillator with a homogeneous or only slightly inhomogeneous distribution of the voltage along the TW part of the structure. We are investigating the details of the operation of such coupled system in this paper.

Two straightforward configurations of the TW waveguides with RTD layers are shown in Fig. 1. In the parallel plate (PP) structure, the bottom metal electrode is fully underneath the RTD layers, whereas for the coplanar waveguide (CPW) structure, a semiconductor heavily-doped (n++) layer stretches underneath the RTD layers, two bottom metal electrodes are placed on both sides of the RTD mesa stripe. These two different structures require different fabrication techniques, since the RTD epilayers are grown on semiconductor substrates. The fabrication of PP structures require a substrate-transfer process [16], which is a more complicated task, compared to top processing needed for CPW structures. The two structures have different characteristics in the terms of waveguide losses and mode properties and that leads to their different frequency limitations, although the overheating problems also impose restrictions on the structure dimensions. Our analysis in the rest of the paper is focused on the structures with PP waveguides.

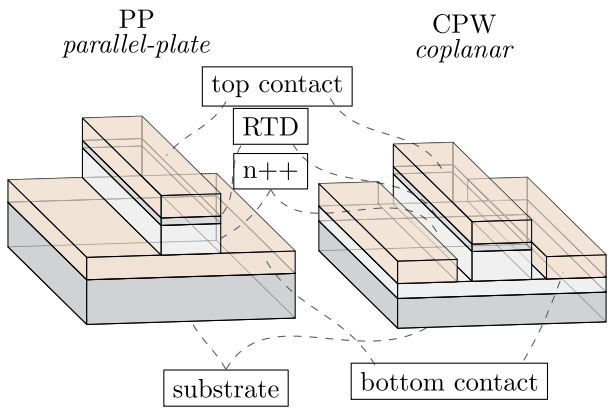

Fig. 1. Two different waveguide geometries. On the left side, the parallel-plate (PP) structure is depicted, where the RTD layers (together with the contact n++ layers) are sandwiched between two metal stripes. On the right side, the coplanar waveguide (CPW) geometry is shown, where the side metal stripes are contacting the bottom n++ layers of RTD.

III. Theory

The TW RTD oscillators are analyzed in three steps. First, the eigen modes of the TW part of the oscillator are analyzed, assuming an infinitely-long waveguide. The objective is to find out, under which conditions the RTD layers provide enough amplification to guarantee a mode gain in the TW waveguide. As the second step, we terminate a finite-length section of the TW waveguide by lumped-element impedances and analyze the eigen resonances of such system in several limiting cases. In the third step, a complete TW RTD oscillator is analyzed, when we take into account, that the termination impedances describe the external part of the system (in particular, an antenna) with additional eigen resonances. The interplay between the internal (TW part) and external (antenna part) resonances is analyzed. Note, the lumped-element RTD oscillators are included in this analysis as a limiting case, when the mode wavelength is large compared to the length of the TW part.

A. Transmission Line Method

Transmission-line method can be used for the analysis of the TW waveguide, assuming that all lateral dimensions of the waveguide are small compared to the eigen-mode wavelength. The TW waveguide can be described by the equivalent circuit [14] shown in Fig. 2. The specific inductance and resistance per unit length of the waveguide are L, and R_{metal}, both of them depend on the operating frequency due to the skin effect. The RTD contact impedance and that of the n++ layers could be described with simple frequency-independent RC parameters. Here one assumes that the skin penetration depth in the n++ layer is much larger than its thickness. Otherwise, one needs to take into account an additional inductive and resistive longitudinal contributions of the n++ layers [17]. The impedance of the RTD layers has a complicated frequency dependence; however, it could be also represented as an RC circuit, although with frequency-depended parameters. For example, one can use the following linear (small-signal) RTD models [18], [19], [20] or a

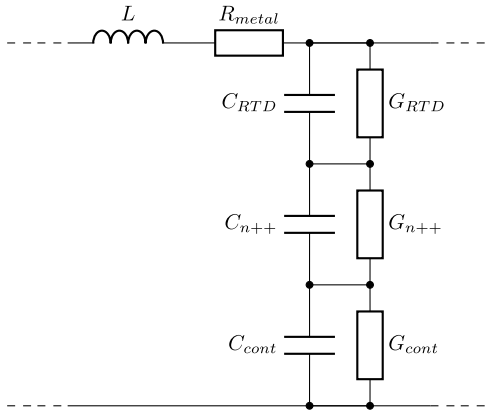

Fig. 2. Equivalent circuit of the TW waveguide.

high-frequency non-linear model [21] for the description of the impedance of the RTD layers.

With the above approximations, the propagation constant k and the wave impedance Z of the TW waveguide mode are:

$$k^2 = XY \qquad Z^2 = \frac{X}{Y} \tag{1}$$

where:

$$X = R_{metal} + i\omega L$$

$$\frac{1}{Y} = \frac{1}{i\omega C_{\mathrm{RTD}} + G_{\mathrm{RTD}}} + \frac{1}{i\omega C_{n++} + G_{n++}} + \frac{1}{i\omega C_{\mathrm{cont}} + G_{\mathrm{cont}}}. \tag{2}$$

The contributions of the n++ layer and the contact resistance could be combined together as a parasitic impedance $Y_p^{-1} = (i\omega C_{n++} + G_{n++})^{-1} + (i\omega C_{\mathrm{cont}} + G_{\mathrm{cont}})^{-1}$.

If one assumes that the operating frequency (f_{op}) lies between 100–500 GHz, the parameters for the contact conductance and capacitance are ($G_{\mathrm{cont}} = g_{\mathrm{cont}} \cdot w$, $g_{\mathrm{cont}} = 1/r_c$, where $r_c \approx 1.5\ \Omega\mu\mathrm{m}^2$ [22], $C_{\mathrm{cont}} = c_{\mathrm{cont}} \cdot w$, $c_{\mathrm{cont}} = 14$ fF/um^2, where w is the width of the waveguide) [23]. The imaginary part of the contact resistance can be neglected at lower frequencies. At higher frequencies (from $\simeq 2$ THz), the imaginary part is going to be the leading term. Similarly, at lower frequencies and thicker n++ layers, the imaginary part of the admittance of the n++ layer can be neglected compared to the real part. The parasitic admittance can be then approximated at low frequencies as:

$$Y_p^{-1} = G_{\mathrm{cont}}^{-1} + G_{n++}^{-1}. \tag{3}$$

Substituting the approximation into (2), we get a low-frequency approximation for the propagation constant:

$$k^2 = (R_{metal} + i\omega L)\left(i\omega C_{RTD}\left(\frac{Y_p}{Y_p + G_{RTD}}\right) + G_{RTD}\right) \cdot \times \left(\frac{Y_p}{Y_p + G_{RTD}}\right). \tag{4}$$

Here it was assumed, that $|Y_p|$ is much larger than the conductance of the RTD layers.

The specific resistance (per unit length along the waveguide) of the metal and the specific inductance of the PP waveguide can be written as:

$$R_{metal} = \frac{2}{w}\sqrt{\frac{\omega\mu_0}{2\sigma}}, \tag{5}$$

$$L = \frac{\mu_0}{w}\left(d_{wg} + 2 \cdot \sqrt{\frac{2}{\omega\sigma\mu_0}}\right), \tag{6}$$

where $\omega = 2\pi f_{op}$, and σ as the conductance of the metal waveguide plates.

We can approximate the specific conductance of the n++ layers as:

$$G_{n++} = \sigma_{n++}\frac{w}{d_{n++}}, \tag{7}$$

where d_{n++} is the thickness of the n++ layers, if we neglect the fringing fields around the PP waveguide. An extension of this model to the CPWs (we are not covering that in this paper) can be not straightforward due to more complicated current paths, which are depending on the CPW geometry, conductances of the layers and contact resistances; stray capacitance can also be giving a significant contribution and it might have a complicated frequency dependence.

The maximum operating frequency of the active TW waveguide could be defined as the frequency where the gain (the real part of the propagation constant) disappears:

$$0 \equiv Im(k^2) = C_{RTD}R_{metal} \cdot \frac{Y_p}{Y_p + G_{RTD}} + LG_{RTD}. \tag{8}$$

Since both expressions for L and G_{n++} include the spacing between the waveguide plates, the two values are coupled. For higher inductance of the waveguide plates, the maximum frequency gets higher, but for lower G_{n++} the losses increase in the structure, decreasing the maximum frequency. According to these considerations, an optimum d_{wg} should exist for the maximum operating frequency. CPW can have advantages over the PP waveguide geometry for certain epilayer structures, since the d_{wg} is not defined by the thickness of the epilayer stack and G_{n++} is defined by different parameters than those in (7).

B. Finite-Length Waveguide

In a realistic geometry, the active waveguide has a finite length and it is coupled to the external environment through the end facets, which we can represent with termination impedances, see Fig. 3. The resonance condition for the system is then:

$$e^{2kl}r_+r_- = 1 \tag{9}$$

$$r_- = \frac{Z_- - Z}{Z_- + Z} \qquad r_+ = \frac{Z_+ - Z}{Z_+ + Z}. \tag{10}$$

Where:

l	length of the waveguide
r_-	reflection coefficient on the left side
r_+	reflection coefficient on the right side
Z_-	termination impedance on the left side

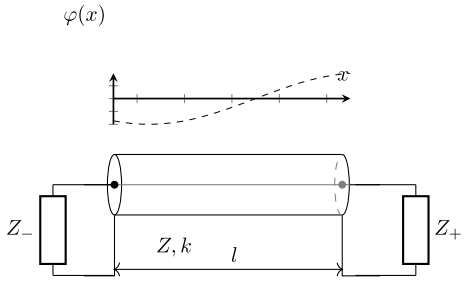

Fig. 3. Finite length (l) waveguide enclosed between Z_+ and Z_- termination impedances.

Z_+ termination impedance on the right side.

We further use the wave-propagation (1)–(7) to find the eigen solutions of (9): G_{RTD} is adjusted to give a real-valued eigen frequencies ω. The voltage distribution between the waveguide plates ($U(x,t)$) corresponds to a standing wave with the amplitude α and could be written in the form:

$$U(x,t) = \varphi(x)\cos(\omega t), \quad \varphi(x) = \alpha(e^{kx} + r_- e^{-kx}). \quad (11)$$

The voltage drop across the RTD layers along the waveguide can be expressed as:

$$\varphi_{RTD}(x) = \varphi(x)\frac{Y_p}{Y_{RTD} + Y_p}, \quad (12)$$

where Y_p is the specific parasitic admittance and $Y_{RTD} = i\omega C_{RTD} + G_{RTD}$ is the specific admittance of the RTD layers.

In order to find the unknown amplitude (α) in (11), one needs to take into account the non-linearity of the RTD I-V curve, since the oscillation amplitudes in RTD oscillators are eventually limited by the RTD non-linearity. In the following analysis, we use a 3rd-order non-linear approximation for the RTD I-V curve, which gives the following equation for the RTD conductance (per unit area): $g(u) = a + 3bu^2$, where a and b are the linear and non-linear parameters of the RTD layers. An effective RTD conductance G_{RTD}, see the equivalent circuit in Fig. 2, at the oscillation frequency (ω) will be a function of the oscillation amplitude (α). We define G_{RTD} based on the power balance considerations: the power generated in the waveguide due to an effective linear G_{RTD} (first harmonic) must be equal to the power generated in RTD layers with account of the RTD non-linearity, i.e.,

$$\begin{aligned}&\int_0^T\int_0^l |\varphi_{RTD}(x)|^2 \cos^2(\omega t)\, G_{RTD}\, dxdt \\ &= \int_0^T\int_0^l |\varphi_{RTD}(x)|^2 \cos^2(\omega t)\, a\, w\, dxdt \\ &\quad + \int_0^T\int_0^l |\varphi_{RTD}(x)|^4 \cos^4(\omega t)\, 3b\, w\, dxdt, \end{aligned} \quad (13)$$

where $T = 2\pi/\omega$ is one oscillation period. Then the power delivered by the system to the terminal impedances Z_+, Z_- will be:

$$\begin{aligned} P_+ &= Re\left(\frac{1}{2Z_+}\right)|\varphi(x)|_{x=l}|^2, \\ P_- &= Re\left(\frac{1}{2Z_-}\right)|\varphi(x)|_{x=0}|^2. \end{aligned} \quad (14)$$

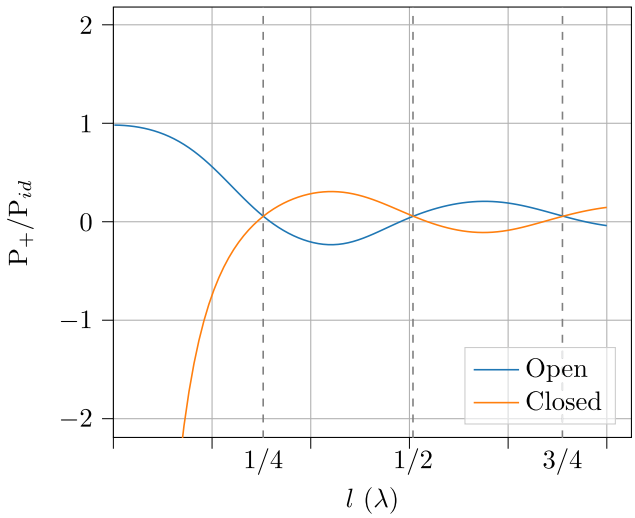

Fig. 4. The relative power output for short-circuit terminated and open-ended waveguides compared to an lumped element oscillator.

To simplify the further analysis, we assume Z_- to be $\{0, \infty\}$, which corresponds to a short-circuit or open termination of the TW waveguide at $x = 0$. With given parameters, the power out-coupled from the system at the Z_+ termination impedance, if it is adjusted to fulfill the resonance condition of (9), is plotted in Fig. 4. P_{id} corresponds to such output power where the voltage distribution on the RTD stripe is homogeneous, that is a limit of a lumped-element RTD oscillator. The two curves represent the short-circuit terminated and open-ended waveguide at the Z_- terminal. The wavelength is defined as $\lambda = 2\pi/Im(k)$. It is important to point out that the negative power corresponds to such structures, which can not be brought to steady-state oscillations by the NDC of the RTD in the device. Hence additional power should flow into the device to match the resonance conditions. It corresponds to termination impedances where the real part of the impedance of the external system is negative (see (14)). If one neglects the parasitics in series with the RTD layers ($Y_p \gg Y_{RTD}$), one ends up with simple relations:

- The open-ended waveguide is equivalent to the lumped element oscillator, $G_{RTD}l = Re(Z_+^{-1})$, when the wavelength is large compared to the waveguide length.

$$P_+ = -2\frac{Re(Z_+^{-1}) + a \cdot lw}{3blw} Re(Z_+^{-1}). \quad (15)$$

- If the waveguide is very long compared to the wavelength, then the wave amplitude will eventually become saturated. In this case, the mode gain is zero, i.e., the RTD gain is exactly compensating for the waveguide losses. This situation is described by (8), which leads to the condition $G_{RTD} \approx -R_{metal}\, C_{RTD}/L$. If we then adjust the

waveguide length in such a way, that the standing-wave resonance condition is satisfied, and if we attach a sufficiently large load resistor (R_+) to the open end of the waveguide ($R_+ \gg |Z|$, so that $r_+ \approx 1$), then the output power generated on the load becomes independent of the waveguide length:

$$P_+ = \frac{2}{3}\frac{G_{RTD} - a\,w}{b\,w}\frac{1}{R_+}. \tag{16}$$

The situation is somewhat similar to lasers with saturated gain and strong back reflection at the end facets.

From these theoretical considerations, an RTD oscillator could be treated as a simple lumped-element oscillator, when the voltage distribution along the RTD mesa is homogeneous ($k \cdot l \ll 1$). Otherwise, one should consider the voltage inhomogeneity in the RTD mesa and treat the mesa as a waveguide.

In a practical system, one wants to make the system oscillating at a target frequency and to have other eigen frequencies in the system suppressed (attenuated). Particularly critical are the low-frequency parasitic oscillations. To suppress them, the load impedance Z_+ needs to be frequency dependent and have sufficiently low real value at low frequencies. That is usually achieved with an additional shunt resistor connected to an RTD oscillator.

When the lateral dimensions of the waveguide getting comparable to the wavelength, the transmission-line methods fails, one needs to use 2D (in the RTD cross section) simulation methods in this case.

C. Full System

Now we take into account the details of the termination impedances, specifically that Z_+ describes an external antenna, which can behave either as a resonator or predominantly as an inductance, if the antenna is operated at frequencies much lower than its eigen frequency. We still consider the situation, when the waveguide is open-ended at one end ($Z_- = \infty$).

In the beginning, we consider a limiting case, when the wavelength is large compared to the TW waveguide length ($|kl| \ll 1$). Linearizing (9), (10), we get the following equation describing the eigen frequencies of a lumped-element RTD oscillator:

$$Z_+ = \frac{Z}{kl}. \tag{17}$$

If the antenna impedance Z_+ can be approximated as that of an inductance ($i\omega L_{ant}$), the resonance frequency of the lumped-element oscillator is:

$$\omega = \frac{1}{\sqrt{L_{ant} C_{RTD} l}}, \tag{18}$$

which behaves as $\omega \propto 1/\sqrt{l}$ with the variation of the length of the TW waveguide, we keep the antenna inductance constant.

In another limiting case of a purely TW oscillator, we assume $Z_- = \infty$ and keep Z_+ as a frequency-independent constant. In this case, (9) and (10) are reduced to

$$Z_+ = \coth(kl) Z. \tag{19}$$

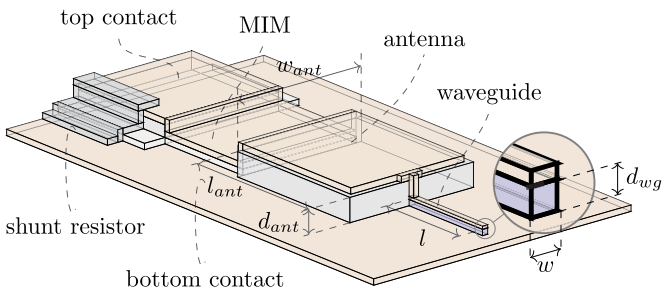

Fig. 5. Geometry of the coupled system with a quarter-wave patch antenna. The parameters for the numerical calculations can be found in Appendix.

The solution of the equation is $kl = const$, which leads to the dependence $\omega \propto 1/l$, assuming a linear $k(\omega)$ dispersion. In practice, the oscillator in the regime $|kl| \sim 1$ is operating in a mixed mode, since Z_+ is frequency dependent and the (resonant) properties of the external parts of the system significantly influence the eigen frequencies of the system.

a) Resonance frequencies of the coupled system:

We construct a model coupled system as shown in Fig. 5. An open-ended TW waveguide is connected to a patch antenna on the other end. The opposite side of the patch antenna should be connected to a MIM. If the wave impedance of the MIM is much smaller than the wave impedance of the patch antenna, then the system acts as a quarter-wave patch antenna.

In the low-frequency limit, the (quarter-wave) patch antenna behaves as an inductance (at frequencies much lower than the antenna resonance frequency) and the TW part behaves as a lumped-element RTD ($|kl| \ll 1$), then the system is in the lumped-element oscillator regime, (18). In the general case, we can write the resonance conditions as:

$$\frac{Z_c}{Z} = \tan(kl)\tan(k_c l_c), \tag{20}$$

where Z_c, k_c, l_c describe the wave impedance, the propagation constant and the length of the patch. The whole system can be seen as two waveguide subsystems coupled together through the Z_c/Z coupling coefficient. One can argue similarly for the half-wave patch antenna system, if no MIM is connected at the other end of the patch:

$$\frac{Z_c}{Z} = \tan(kl)\tan\left(k_c l_c - \pi/2\right), \tag{21}$$

Qualitatively, the resonance frequencies of the quarter-wave patch antenna system as the function of the length of the TW RTD waveguide are plotted in Fig. 6 with the parameters given in Table I (see Appendix). The continuous and dashed curves represent the resonant frequencies of the coupled system, while the dotted lines show the resonant frequencies of the uncoupled subsystems ($Z/Z_c = \infty$ or 0). As the two systems get coupled, the RTD waveguide is not working as a pure (isolated) TW oscillator anymore, but as an oscillator which is a mixture of the characteristics of the two systems. The right axis in Fig. 6 shows the required NDC (provided by RTD) to maintain the stationary oscillation conditions. The quarter-wave resonances of the decoupled patch antenna and TW RTD are crossing at

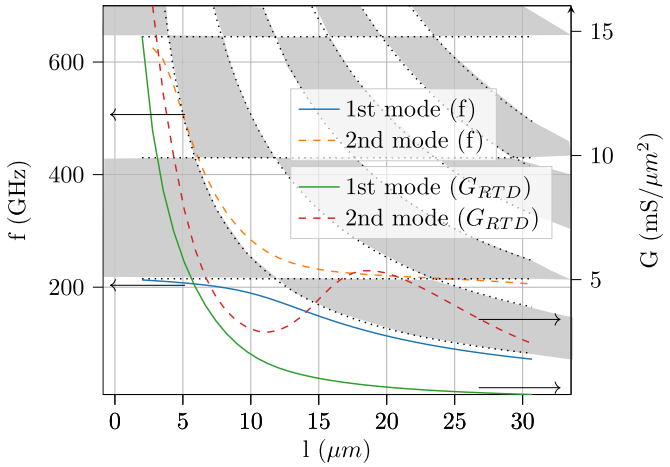

Fig. 6. Two lowest oscillation modes in a TW RTD coupled to a "quarter-wave" patch antenna plotted as frequency vs. TW-waveguide length. The RTD and antenna parameters are given in Table I. The right axis gives the minimal value of RTD NDC (G_{RTD}) needed to satisfy the oscillation conditions. The doted horizontal lines show (with increasing frequency) $\lambda/4$, $\lambda/2$, and $\lambda 3/4$ eigen resonances in the stand-alone patch antenna. The $1/l$ doted lines show (with increasing frequency) $\lambda/4$, $\lambda/2$, $\lambda 3/4$, etc. eigen resonances in the stand-alone TW RTD. The forbidden regions, where no oscillation are possible, are plotted in gray.

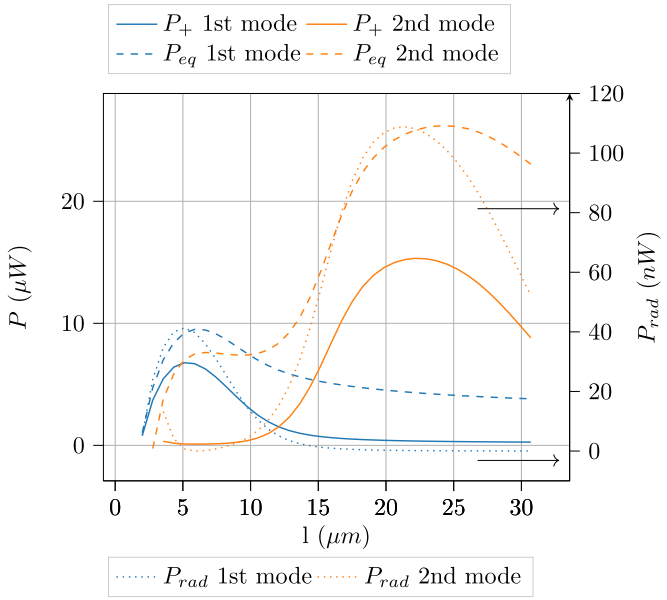

Fig. 7. The output power of two lowest resonant modes of the model coupled system. The plot also shows the equilibrium (P_{eq}) and the radiated powers.

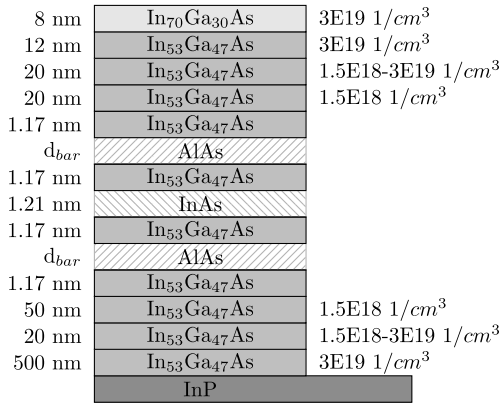

Fig. 8. RTD epilayers, specifying the layer thicknesses and the dopinglevel. The d_{bar} represents the thickness of RTD barriers.

$\approx 200\,\text{GHz}$ for $l \approx 12\,\mu\text{m}$, therefore the resonance modes of the coupled system are exhibiting an anti-crossing behavior around this point. Namely, for shorter TW RTDs ($\lesssim 12\,\mu$m), the first mode behaves as a lumped-element RTD oscillator with a quarter-wave patch resonator, whereas the second mode behaves as a quarter-wave TW RTD resonator ($\propto 1/l$). For longer RTD lengths ($\gtrsim 12\,\mu$m), the behavior character of the two modes is flipped.

One can interpret the properties of the resonant modes of the coupled system as a resonance of two (patch and TW RTD) coupled sub-systems: in the resonance, one sub-system should behave as a capacitance (with positive susceptance), while the other one as an inductance (negative susceptance). At frequencies below the quarter-wave resonances of the sub-systems, the patch antenna behaves as an inductance, whereas the TW RTD as a capacitance. After crossing the $\lambda/4$, $\lambda/2$, $\lambda 3/4$, etc. resonances, the behavior of each of the sub-systems is sequentially flipped. That leads to the allowed regions for the resonance modes of the coupled system in the spectrum, where the resonance modes are lying, that are white areas in Fig. 6. However, no resonance modes are possible in the regions, where both sub-systems behave as capacitances or inductances simultaneously, those forbiden regions are shown in gray color in Fig. 6.

b) Output power of the coupled system:

The output power of the example system is plotted in Fig. 7. For small TW waveguides (with approximately $l < 3\,\mu m$), RTD NDC is not sufficient to compensate for the losses in the coupled system, that corresponds to a negative output power, we skip those points in Fig. 7. On the other hand, the first mode is less suitable to emit power due to a low voltage amplitude on the Z_+ termination impedance. In this case, the system is to large extend dissipating the power in the metallization of the TW waveguide and in the n++ layers. P_{eq} in Fig. 7 represents the total power generated by the RTD layers, it is defined as the integrals on both sides in (13).

On the other hand, the second mode has stronger emission for longer TW stripes with $l \approx 23\,\mu$m, see Fig. 7. That corresponds to a quarter-wave resonance (with high radiation efficiency) in the patch antenna and a half-wave resonance in the TW RTD, see spectrum in Fig. 6. This resonance is also seen as a smooth peak for G at $l \approx 20\,\mu$m in Fig. 6.

The emitted power from the rectangular patch antenna can be calculated based on [24]. Here, the radiation losses are much lower than the conduction losses in the system, implying the radiated power can be calculated simply by multiplying the power output of the waveguide by the radiation efficiency of the antenna. However, the width of the antenna used in this calculation is much smaller than the MIM width (see Fig. 10), the

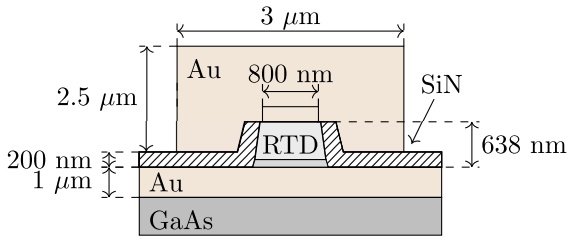

Fig. 9. Cross-section of the PP waveguide. The dashed areas are SiN layers, the areas indicated with brown color are the metallization layers.

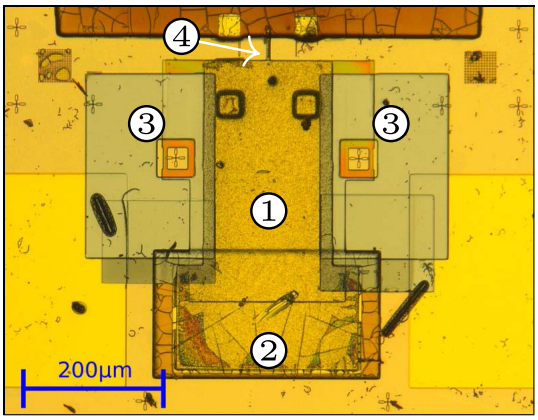

Fig. 10. Image of the fabricated PP-waveguide oscillator with MIM as antenna. In the picture the different parts of the device are labeled: **1** - MIM, **2** - Top contact, **3** - Shunt resistor, **4**- RTD stripe.

MIM capacitor is capable of radiating some power as well, hence our calculations give a conservative estimate for the radiated power.

IV. Fabrication

Several different oscillators were fabricated using both CPW and PP waveguide structures. The CPW structures proved to have limitations due to the lack of cooling around RTDs, they overheated for our RTD-wafer parameters and oscillator geometry. In this work, just the structures with PP waveguides are presented. For comparison, we fabricated our devices based on two different RTD wafers (with 1.4 nm and 1.8 nm RTD-barrier thicknesses). The complete RTD substrate layer stack is shown in Fig. 8. Detailed information on similar RTDs with 1.6 nm barriers has been presented in [25]. The PP waveguide cross section of our devices is shown in Fig. 9.

Wafer bonding: In order to lower the temperature of the RTD mesa, one needs to have better heat conduction between the RTD and the substrate. Therefore, the substrate transfer process has been used and a thick metal heat-conductor layer was introduced between the epilayers and the substrate [16]. The new substrate material was undoped GaAs which was slightly larger than the InP sample (10x10 mm). Prior to the bonding process, the two surfaces were cleaned (contact cleaning with 10% HCl solution for 30 s) and the metallization layers with Ti(10 nm)/Au(500 nm) were sputter deposited on both surfaces. In the bonding process, the surfaces were pushed together with 450 N for 30 minutes at 330 °C and were let to cool down slowly. The full 500 μm thick InP substrate was etched away with concentrated HCl solution. It was important to scratch the surface of the InP substrate since the polished side is not etched by HCl. The HCl selectively etched InP with respect to the arsenic layers, hence the well timed removal of the samples from the enchant was not necessary.

From the formed metal sandwich, the RTD TW waveguides were fabricated using dry etching in $CH_4/H_2/Ar$ plasma, using a negative photo resist as a mask. For the passivization of the surface of the RTD and as a dielectric layer for MIM capacitor, 200 nm SiN was deposited with PECVD process. In the fabricated samples, the TW waveguide was directly connected to the MIM section. The MIM was formed by a thin novolak ($\sim$ 300 nm cross-linked novolak resist [26]) layer on top of SiN. Further on, an additional thick (1.5 μm) novolak layer for mechanical stability was fabricated under the contact pad. The top metallization was thickened by electroplating in order to increase the heat conduction around the RTD waveguide, while the shunt resistor is formed by sputter-deposited Ti. It was important to have large surface area shunt resistors for the devices since they have to dissipate around a 1 W of power. An image of the fabricated oscillator is shown in Fig. 10.

V. Analysis of the Fabricated Devices

To force the oscillator to be working in the TW regime, we have excluded the patch antenna from our design, we made the TW section to be directly connected to the MIM, which should ideally be functioning as a short-circuit termination for the TW waveguide (the waveguide remains open on the other end). The other way to see our design: we tried to shift the resonance frequencies of the external (patch-antenna) system as high as possible, by reducing the length of the patch and eventually eliminating it in order to minimize its influence on the eigen TW-waveguide resonant modes. In practice, however, the MIM impedance has a rather complicated frequency dependence with several eigen resonances. Therefore, the MIM behaves rather as as a large patch antenna (with a low input impedance though!) with a small separation between the patch and the ground plane and with an additional loading by a parallel shunt, see Fig. 10.

A. Numerical Calculation

To analyze the behavior of such TW RTD oscillator quasi-shortcircuited by the MIM, we have numerically calculated the impedance of the MIM (Z_+) and then calculated the eigen modes of the oscillator with (19). The input MIM impedance is low (MIM is also directly connected to a distributed shunt of 1 Ω) compared to the wave impedance of the TW RTD stripe, however, it has a complicated frequency dependence: it behaves as a lossy inductance bellow $\approx$ 180 GHz (dotted horizontal line in Fig. 11), then as a lossy capacitor up to $\approx$ 300 GHz (the next dotted horizontal line) and then again as a lossy inductance. That approximately defines the forbidden and allowed regions in the spectrum in Fig. 11.

However, contrary to the case of a high-impedance (low-loss) quarter-wave patch shown in Fig. 6, the mode structure in the

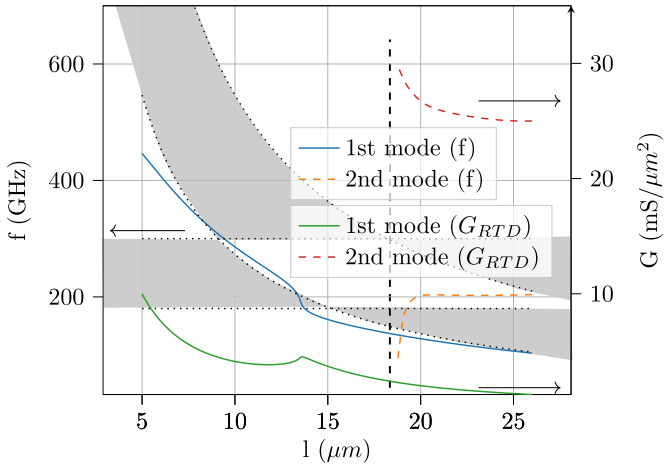

Fig. 11. The resonant frequency of the antennaless TW RTD system is plotted as the function of the TW waveguide length. G_{RTD} (right axis) gives the minimal NDC values that satisfy the resonance (oscillation) conditions. The resonant frequencies of the unperturbed systems (two decoupled waveguides) are plotted as dotted lines. The forbidden regions, where no oscillation are possible, are plotted (qualitatively) in gray.

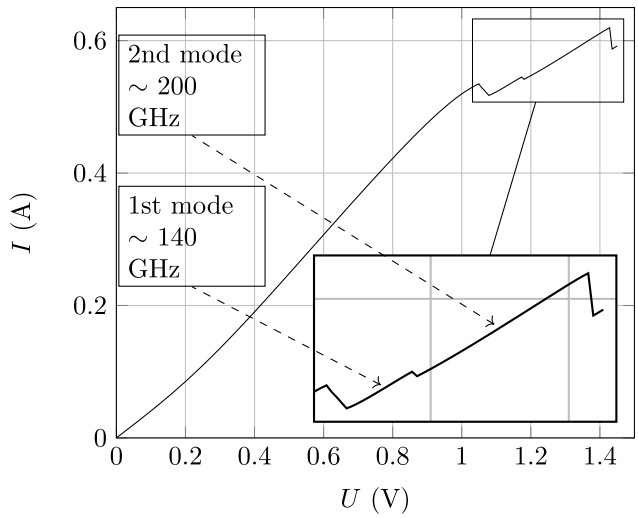

Fig. 12. IV curve (with shunt) of a TW oscillator connected directly to MIM with TW-section length of 22.5 μm, the RTD had the barriers of 1.4 nm.

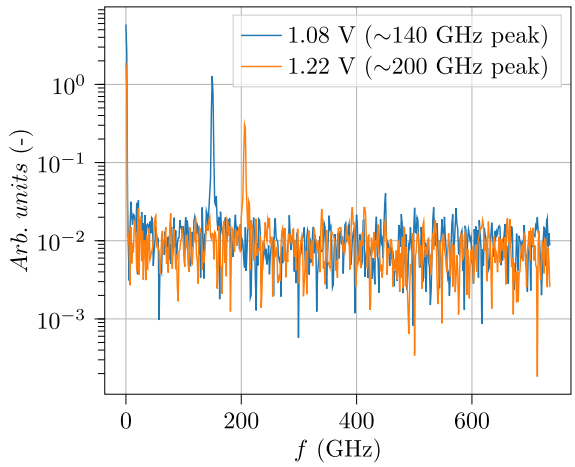

Fig. 13. Output spectra of the device which IV curve is plotted in Fig. 12 for two different bias points with different oscillation modes.

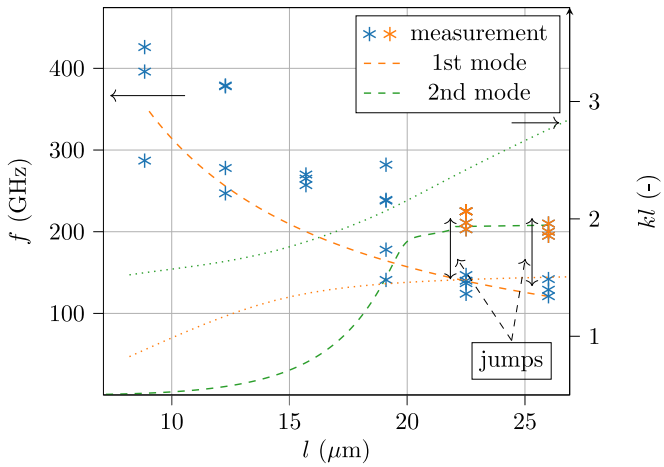

Fig. 14. Frequency vs. RTD-stripe length for a TW RTD oscillator with a MIM termination, RTD layers are with 1.4 nm barriers. The dotted lines show the $|kl|$ parameter for the TW waveguide.

TW RTD oscillator loaded by MIM is qualitatively different. In this case, the anti-crossing behavior (seen in Fig. 6) and the lumped-element resonance are suppressed due to high attenuation in the MIM. The system behaves now as almost pure TW RTD resonator perturbed by the (low) MIM load impedance. The lowest mode in the system corresponds now to the quarter-wave resonance in the TW RTD (as intended), it approximately follows the $\propto 1/l$ line. The deviations of the spectrum from this line are due to the inductive or capacitive character of the MIM termination impedance: the spectrum shifts, correspondingly, a bit below or above $\propto 1/l$ line, see blue line in Fig. 11. The second mode corresponds to half-wave resonance in the TW RTD, which is connected to a high-loss MIM resistance. This mode appears only for longer RTD stripes of more than $\approx 20\ \mu$m. In principle, this second mode should not appear, if MIM would have zero impedance, but it does show up in our system due to a not sufficiently low MIM impedance.

B. Measurements

The radiation we measure in our devices was generated by the TW part directly and partly as a parasitic radiation of the open edges of MIM. The oscillation frequency of our samples was measured with a Martin–Puplett interferometer with a Golay cell as a detector; the interferometer covers continuously the frequency range from ≈50 GHz up to ≈5 THz.

On longer RTD stripes, one can see an additional jump on the IV curve as it is shown in Fig. 12. These jumps correspond to a stepwise change in the oscillation frequency of the oscillator with the bias sweep. The measured radiation spectra to the left and right from a jump (for the very same device) are shown in Fig. 13. The different frequencies on both sides of the jumps (the jumps occur for several devices) are shown as orange and blue points in Fig. 14.

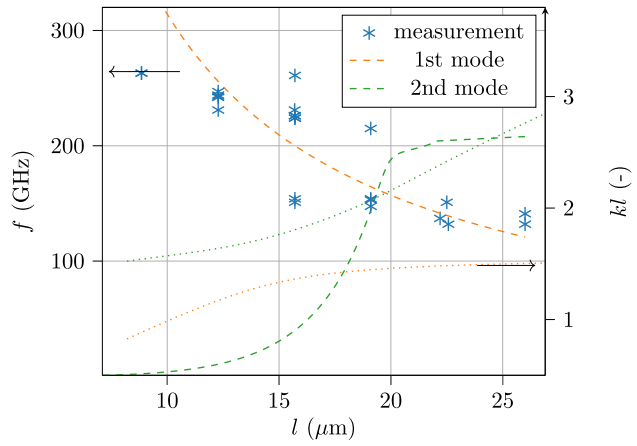

Fig. 15. Frequency vs. RTD-stripe length for a TW RTD oscillator with a MIM termination, RTD layers are with 1.8 nm barriers. The dotted lines show the $|kl|$ parameter for the TW waveguide.

Qualitatively, one explains the appearance of the jump in the following manner: as the RTD voltage is increased, the capacitance of the RTD decreases – leading to a high wave-propagation speed – effectively resulting in a smaller $|kl|$ parameter, that needs to be compensated by an increase in frequency, which at some point results in switching between the 2nd- and the 1st-mode resonances in the system. Another important factor is the frequency dependence of the termination MIM impedance (with internal damped eigen resonances), which also could be making the switching between two resonant modes favorable, see Fig. 11. The position of 1st and 2nd modes can be estimated by assuming constant capacitance and weak non-linearity in the system (see Section III-C). On the other hand, the mode switching (or mode selection) between these two modes can not be described with these simple assumptions. Generally, the phenomenon can be seen as a behavior of coupled non-linear microwave circuits [27] whereas the changing of the non-linearity affects the stability of the oscillation modes in the structure; detailed analysis of the mode selection mechanism goes beyond the scope of the paper.

The frequency vs. TW-waveguide length relation is plotted in Fig. 14 for 1.4 nm barrier RTDs. The frequency measurement points are the averaged frequency points since the oscillation frequency continuously changes with the bias voltage in each plateau of the IV curve. One can separate the measured frequency points into two curves which come from the 1st and 2nd modes of the system. In Fig. 14, the jumps indicate two different measured operating frequencies of the devices, which have the I-V curves with jumps, as plotted in Fig. 12. The measured spectra of a device, which exhibits operating-frequency jumps as a function of the bias, are plotted in Fig. 13 for two bias points.

A similar argument could be made for the measurement for the 1.8 nm barrier RTD which is plotted in Fig. 15. For devices that possess lower specific NDC (with 1.8 nm barriers), the frequency jumps do not occur; the system oscillates just in one or in the other mode. The probable reason is that these RTDs, due to their lower NDC, induce lower non-linearity in the system, that is why the Hopf-bifurcations do not occur.

In Figs. 14, 15, the phase $|kl|$ parameter in the TW RTD waveguide is plotted. It shows that the switching occurs, when the phase parameter gets close to $\pi/2$ (i.e., to the quarter-wave condition for the TW waveguide), then the switching to the second mode happens.

A general comment with outlook. The analysis of the waveguide losses in the TW section of our devices indicates, that the dominant loss mechanism (at least at lower frequencies, see also [14]) could be attributed to the skin-effect losses in the metal, see (8). This effect can be lowered by reducing the specific capacitance of the waveguide, which is mainly the specific capacitance of the RTD layers. That would require a design of the RTD layers with a thick depletion layer and possibly with a reduced quantum-well RTD capacitance. Such TW waveguide would have a cross section closer to that of the metal-metal QCL waveguides, where the gain layers fill almost the whole space between the metal stripes. However, the electron transport times through the thick depletion RTD layers may limit the applicability of the concept to lower sub-THz frequencies.

VI. Conclusion

A coupled system consisting of a TW RTD section and an external patch antenna has been analyzed theoretically. We show, that some eigen resonances in the system could be attributed to the lumped-element resonances, the others are closer to the eigen resonances in the TW section of the structure, but in general it is essential to treat the system as a coupled one with the eigen modes and eigen resonances distributed between both subsections of the system. We provide a proof-of-principle experimental demonstration of the TW RTD oscillators. The oscillators were working in the frequency range 100-400 GHz and the TW section was operated close and above the quarter-wave regime. We also demonstrate that some oscillators were switching between different resonant modes of the system with the change of bias. The phenomenon could be used for extended frequency control of the RTD oscillators and perhaps for frequency modulation.

The RTD epilayers studied experimentally and used for quantitative assessments in the paper are not optimized for TW type of RTD oscillators. Further optimization of RTD epilayers and parameters of TW waveguide and emitting antenna should enable better performance TW RTD oscillators.

VI. Acknowledgment

Regarding the fabrication, ZJ would like to thank the employees of the CEITEC Nano Institute for their enormous help. We would like to thank also Petr Ouředník for the helpful comments and discussions.

Appendix

A. Model Device

In Section III-C a traveling-wave RTD oscillator with a quarter wave patch antenna was analyzed. The parameters of the device used in the numerical calculation are given in Table I.

TABLE I
THE NUMERICAL PARAMETERS USED FOR SIMULATION OF THE COUPLED SYSTEM

Symbol	Parameters Description and unit	Value
l	length of the waveguide [μm]	2-40
a	Small signal NDC of RTD substrate [$\mathrm{mS}/\mu\mathrm{m}^2$]	16
b	Large signal NDC non-linearity of the RTD substrate [$\mathrm{mS}/\mu\mathrm{m}^2\mathrm{V}^2$]	21
w	width of the waveguide [μm]	1
σ	conductivity of metalization [$\mathrm{S\,m}^{-1}$]	$2 \cdot 10^7$
d_{wg}	thickness of RTD substrate [nm]	600
c_{RTD}	areal capacitance of RTD [$\mathrm{fF}/\mu\mathrm{m}^2$]	8.5
ρ_{cont}	($\equiv 1/g_{cont}$) contact resistance [$\Omega\mu\mathrm{m}^2$]	10
w_{ant}	antenna width [μm]	200
l_c	antenna length [μm]	200
d_{ant}	antenna thickness [μm]	0.5

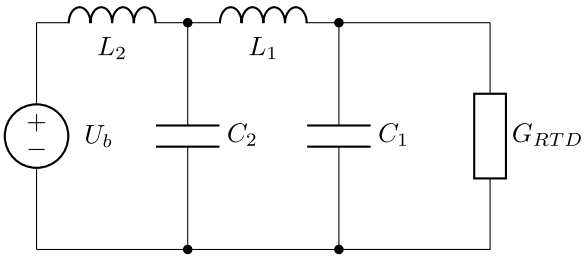

Fig. 16. Equivalent picture of an RTD oscillator with multiple resonant modes.

B. Bifurcations in the Non-Linear System

In most resonator structures, multiple different modes can oscillate. It was shown in Section III-C and with the measurements that two different modes can be excited in the presented system. Some of the devices with 1.4 nm barrier thickness presented different oscillation frequencies upon changes the bias voltage (see Figs. 12, 14). The analysis of switching between the two possible oscillation modes can be better understood and analyzed with a simplified model in which a series and a parallel LC resonant circuits are coupled (see Fig. 16). The proposed circuit has two resonant modes in which the voltage is in phase or in anti-phase on the capacitors - this is the same as in the traveling-wave oscillator - comparing the voltage at the MIM and at the RTD. The first mode can be called common-mode, as the voltage on the MIM and on the RTD are in phase. While in the 2nd mode, an additional node appears, and the two parts of the system are in anti-phase. As the U_b bias voltage changes, the system may jump from one mode to the other one or create a more complicated oscillatory behavior depending on the non-linearity [28].

C. Measurement Setup

The spectra of the devices were measured with a Martin-Pupplet interferometer, based on the work of [29], see schematic in Fig. 17.

In order to measure the power of the RTD oscillator selectively with the setup, additional filtering should be used. The bias voltage of the RTD was chopped with a reasonable low frequency (≈17 Hz), and the detected power on the detector was filtered for this chopping frequency with a lock-in amplifier. A Golay-cell was used as a detector for this setup. The chopping

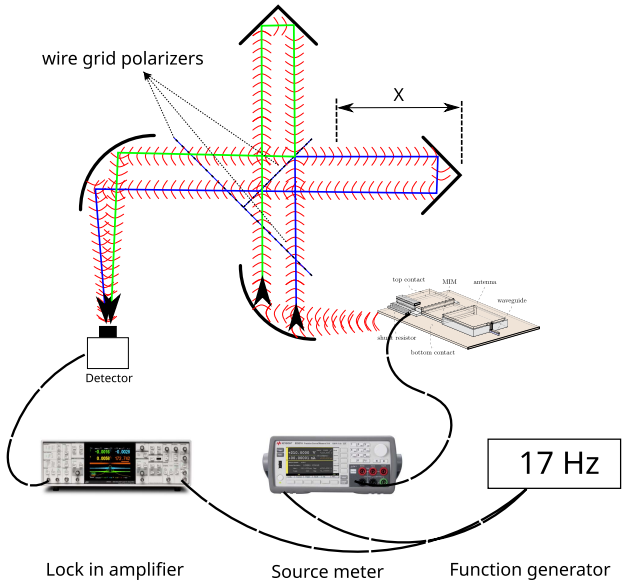

Fig. 17. Schematics of the interferometer setup.

frequency was chosen to have minimal interference with the surrounding (≈50 Hz) sources, low enough to be in the detector's response time limitations and high enough to have reasonable measurement times. In the interferometer, one rooftop mirror was moved during the measurement, and in each step, the filtered signal was measured with the lock-in amplifier. The applied method made it feasible to measure several nW-s in the sub-THz frequency range.

REFERENCES

[1] B. S. Williams, "Terahertz quantum-cascade lasers," *Nature Photon.*, vol. 1, no. 9, pp. 517–525, 2007.
[2] B. S. Williams, S. Kumar, Q. Hu, and J. L. Reno, "High-power terahertz quantum-cascade lasers," *Electron. Lett.*, vol. 42, no. 2, pp. 89–91, 2006.
[3] E. R. Brown, J. Söderström, C. Parker, L. Mahoney, K. Molvar, and T. McGill, "Oscillations up to 712 GHz in InAs/AlSb resonant-tunneling diodes," *Appl. Phys. Lett.*, vol. 58, no. 20, pp. 2291–2293, 1991.
[4] M. Asada and S. Suzuki, "Room-temperature oscillation of resonant tunneling diodes close to 2 THz and their functions for various applications," *J. Infrared Milli. Terahz. Waves*, vol. 37, pp. 1185–1198, Dec. 2016.
[5] M. Feiginov, "Frequency limitations of resonant-tunnelling diodes in sub-THz and THz oscillators and detectors," *J. Infrared Milli. Terahz. Waves*, vol. 40, pp. 365–394, 2019.
[6] R. Izumi, S. Suzuki, and M. Asada, "1.98 THz resonant-tunneling-diode oscillator with reduced conduction loss by thick antenna electrode," in *Proc. IEEE 42nd Int. Conf. Infrared, Millimeter, Terahertz Waves*, 2017, pp. 1–2.
[7] T. Maekawa, H. Kanaya, S. Suzuki, and M. Asada, "Oscillation up to 1.92 THz in resonant tunneling diode by reduced conduction loss," *Appl. Phys. Exp.*, vol. 9, no. 2, 2016, Art. no. 024101.
[8] X. Mei et al., "First demonstration of amplification at 1 THz using 25-nm InP high electron mobility transistor process," *IEEE Electron Device Lett.*, vol. 36, no. 4, pp. 327–329, Apr. 2015.
[9] A. Khalid et al., "A planar gunn diode operating above 100 GHz," *IEEE Electron Device Lett.*, vol. 28, no. 10, pp. 849–851, Oct. 2007.
[10] T. A. Midford and R. L. Bernick, "Millimeter-wave CW IMPATT diodes and oscillators," *IEEE Trans. Microw. Theory Techn.*, vol. 27, no. 5, pp. 483–492, May 1979.
[11] M. Feiginov, R. Gonzalo, I. Maestrojuán, O. Cojocari, M. Hoefle, and E. Limiti, "THz electronics," in *Semiconductor Terahertz Technology: Devices and Systems at Room Temperature Operation*. Chichester, U.K.: Wiley, 2015, pp. 254–303.

[12] S. Suzuki, K. Hinata, M. Shiraishi, M. Asada, H. Sugiyama, and H. Yokoyama, "RTD oscillators at 430–460 GHz with high output power (200 μw) using integrated offset slot antennas," in *Proc. IEEE 22nd Int. Conf. Indium Phosphide Related Mater.*, 2010, pp. 1–4.

[13] S. Kitagawa, S. Suzuki, and M. Asada, "Wide frequency-tunable resonant tunnelling diode terahertz oscillators using varactor diodes," *Electron. Lett.*, vol. 52, no. 6, pp. 479–481, 2016.

[14] M. Feiginov, "Sub-terahertz and terahertz microstrip resonant-tunneling-diode oscillators," *Appl. Phys. Lett.*, vol. 107, no. 12, 2015, Art. no. 123504.

[15] M. E. Hines, "High-frequency negative-resistance circuit principles for esaki diode applications," *Bell Syst. Tech. J.*, vol. 39, no. 3, pp. 477–513, 1960.

[16] P. Karbownik et al., "Direct Au–Au bonding technology for high performance GaAs/AlGaAs quantum cascade lasers," *Opt. Quantum Electron.*, vol. 47, no. 4, pp. 893–899, 2015.

[17] Y. R. Kwon, V. M. Hietala, and K. S. Champlin, "Quasi-TEM analysis of "slow-wave" mode propagation on coplanar microstructure MIS transmission lines," *IEEE Trans. Microw. Theory Techn.*, vol. 35, no. 6, pp. 545–551, Jun. 1987.

[18] M. N. Feiginov, "Effect of the coulomb interaction on the response time and impedance of the resonant-tunneling diodes," *Appl. Phys. Lett.*, vol. 76, 2000, Art. no. 2904.

[19] M. N. Feiginov, "Does the quasibound-state lifetime restrict the high-frequency operation of resonant-tunnelling diodes?," *Nanotechnol.*, vol. 11, 2000, Art. no. 359.

[20] M. N. Feiginov, "Displacement currents and the real part of high-frequency conductance of the resonant-tunneling diode," *Appl. Phys. Lett.*, vol. 78, 2001, Art. no. 3301.

[21] M. Feiginov, C. Sydlo, O. Cojocari, and P. Meissner, "High-frequency nonlinear characteristics of resonant-tunnelling diodes," *Appl. Phys. Lett.*, vol. 99, 2011, Art. no. 133501.

[22] A. Baraskar et al., "Ex situ ohmic contacts to n-InGaAs," *J. Vac. Sci. Technol. B., Nanotechnol. Microelectronics: Mater., Process. Meas. Phenomena*, vol. 28, no. 4, pp. C5I7–C5I9, 2010.

[23] N. Orihashi, S. Hattori, S. Suzuki, and M. Asada, "Experimental and theoretical characteristics of sub-terahertz and terahertz oscillations of resonant tunneling diodes integrated with slot antennas," *Japanese J. Appl. Phys.*, vol. 44, no. 11R, 2005, Art. no. 7809.

[24] H. Pues and A. V. de Capelle, "Accurate transmission-line model for the rectangular microstrip antenna," *IEE Proc. H. (Microwaves, Opt. Antennas)*, vol. 131, no. 6, pp. 334–340, 1984.

[25] P. Ourednik, T. Hackl, C. Spudat, D. Tuan Nguyen, and M. Feiginov, "Double-resonant-tunneling-diode patch-antenna oscillators," *Appl. Phys. Lett.*, vol. 119, no. 26, 2021, Art. no. 263509.

[26] M. Drumm, C. Dodge, and L. Nielsen, "Cross linking of a phenol-formaldehyde novolac-determiantion by dynamic-mechanical measurements," *Ind. Eng. Chem.*, vol. 48, no. 1, pp. 76–81, 1956.

[27] A. Suárez and R. Quéré, *Stability Analysis of Nonlinear Microwave Circuits*. Norwood, MA, USA: Artech House, 2003.

[28] F. Ramírez, S. Sancho, and A. Suárez, "Oscillation modes in multiresonant oscillator circuits," *IEEE Trans. Microw. Theory Techn.*, vol. 64, no. 12, pp. 4660–4675, Dec. 2016.

[29] S. Schmuck et al., "Electron cyclotron emission spectra in X-and O-mode polarisation at jet: Martin-puplett interferometer, absolute calibration, revised uncertainties, inboard/outboard temperature profile, and wall properties," *Rev. Sci. Instruments*, vol. 87, no. 9, 2016, Art. no. 093506.